

This is a repository copy of *The role of core excitations in the structure and decay of the 16+ spin-gap isomer in 96Cd*.

White Rose Research Online URL for this paper:

<https://eprints.whiterose.ac.uk/114463/>

Version: Published Version

---

**Article:**

Davies, P. J. [orcid.org/0000-0002-9003-0603](https://orcid.org/0000-0002-9003-0603), Grawe, H., Moschner, K. et al. (45 more authors) (2017) The role of core excitations in the structure and decay of the 16+ spin-gap isomer in 96Cd. *Physics Letters, Section B: Nuclear, Elementary Particle and High-Energy Physics*. pp. 474-479. ISSN 0370-2693

<https://doi.org/10.1016/j.physletb.2017.02.013>

---

**Reuse**

This article is distributed under the terms of the Creative Commons Attribution (CC BY) licence. This licence allows you to distribute, remix, tweak, and build upon the work, even commercially, as long as you credit the authors for the original work. More information and the full terms of the licence here:

<https://creativecommons.org/licenses/>

**Takedown**

If you consider content in White Rose Research Online to be in breach of UK law, please notify us by emailing [eprints@whiterose.ac.uk](mailto:eprints@whiterose.ac.uk) including the URL of the record and the reason for the withdrawal request.



# The role of core excitations in the structure and decay of the $16^+$ spin-gap isomer in $^{96}\text{Cd}$



P.J. Davies<sup>a,\*</sup>, H. Grawe<sup>b</sup>, K. Moschner<sup>c,g</sup>, A. Blazhev<sup>c</sup>, R. Wadsworth<sup>a</sup>, P. Boutachkov<sup>d</sup>, F. Ameil<sup>b</sup>, A. Yagi<sup>e</sup>, H. Baba<sup>g</sup>, T. Bäck<sup>h</sup>, M. Dewald<sup>c</sup>, P. Doornenbal<sup>g</sup>, T. Faestermann<sup>k</sup>, A. Gengelbach<sup>i</sup>, J. Gerl<sup>b</sup>, R. Gernhäuser<sup>k</sup>, S. Go<sup>n</sup>, M. Górska<sup>b</sup>, E. Gregor<sup>d</sup>, T. Isobe<sup>g</sup>, D.G. Jenkins<sup>a</sup>, H. Hotaka<sup>n</sup>, J. Jolie<sup>c</sup>, I. Kojouharov<sup>b</sup>, N. Kurz<sup>b</sup>, M. Lewitowicz<sup>o</sup>, G. Lorusso<sup>g</sup>, L. Maier<sup>k</sup>, E. Merchan<sup>d</sup>, F. Naqvi<sup>j</sup>, H. Nishibata<sup>f</sup>, D. Nishimura<sup>n</sup>, S. Nishimura<sup>g</sup>, F. Nowacki<sup>p</sup>, N. Pietralla<sup>d</sup>, H. Schaffner<sup>b</sup>, P.-A. Söderström<sup>g</sup>, H.S. Jung<sup>n</sup>, K. Steiger<sup>k</sup>, T. Sumikama<sup>l</sup>, J. Taprogge<sup>m</sup>, P. Thöle<sup>c</sup>, N. Warr<sup>c</sup>, H. Watanabe<sup>g</sup>, V. Werner<sup>d,j</sup>, Z.Y. Xu<sup>g</sup>, K. Yoshinaga<sup>g</sup>, Y. Zhu<sup>n</sup>

<sup>a</sup> Department of Physics, University of York, York YO10 5DD, United Kingdom

<sup>b</sup> GSI Helmholtzzentrum für Schwerionenforschung, D-64291 Darmstadt, Germany

<sup>c</sup> Institut für Kernphysik, Universität zu Köln, D-50937 Köln, Germany

<sup>d</sup> IKP, Technische Universität Darmstadt, 64289 Darmstadt, Germany

<sup>e</sup> Research Center for Nuclear Physics, Osaka University, Ibaraki, Osaka 567-0047, Japan

<sup>f</sup> Department of Physics, Osaka University, Toyonaka, Osaka 560-0043, Japan

<sup>g</sup> RIKEN Nishina Center, Wako, Saitama 351-0198, Japan

<sup>h</sup> Department of Physics, Royal Institute of Technology, SE-10691 Stockholm, Sweden

<sup>i</sup> Department of Physics and Astronomy, Uppsala University, SE-75121 Uppsala, Sweden

<sup>j</sup> Wright Nuclear Structure Laboratory, Yale University, New Haven, CT 06511, USA

<sup>k</sup> Physik Department E12, Technische Universität München, D-85748 Garching, Germany

<sup>l</sup> Department of Physics, Tohoku University, 6-3 Aramaki-Aoba, Aoba, Sendai, Miyagi 980-8578, Japan

<sup>m</sup> Instituto de Estructura de la Materia, CSIC, E-28006 Madrid, Spain

<sup>n</sup> Department of Physics, University of Tokyo, Bunkyo, Tokyo 113-0033, Japan

<sup>o</sup> Grand Accélérateur National d'Ions Lourds (GANIL), CEA/DSM – CNRS/IN2P3, F-14076 Caen Cedex 5, France

<sup>p</sup> IPHC, IN2P3-CNRS et Université de Strasbourg, F-67037 Strasbourg, France

## ARTICLE INFO

### Article history:

Received 19 October 2016

Received in revised form 11 January 2017

Accepted 9 February 2017

Available online 14 February 2017

Editor: V. Metag

### Keywords:

$\beta$ -decay

$\beta p$ -decay

$\gamma$ -ray spectroscopy

Half-life

Shell-model

WKB

## ABSTRACT

The first evidence for  $\beta$ -delayed proton emission from the  $16^+$  spin gap isomer in  $^{96}\text{Cd}$  is presented. The data were obtained from the Rare Isotope Beam Factory, at the RIKEN Nishina Center, using the BigRIPS spectrometer and the EURICA decay station.  $\beta p$  branching ratios for the ground state and  $16^+$  isomer have been extracted along with more precise lifetimes for these states and the lifetime for the ground state decay of  $^{96}\text{Cd}$ . Large scale shell model (LSSM) calculations have been performed and WKB estimates made for  $\ell = 0, 2, 4$  proton emission from three resonance-like states in  $^{96}\text{Ag}$ , that are populated by the  $\beta$  decay of the isomer, and the results compared to the new data. The calculations suggest that  $\ell = 2$  proton emission from the resonance states, which reside  $\sim 5$  MeV above the proton separation energy, dominates the proton decay. The results highlight the importance of core-excited wavefunction components for the  $16^+$  state.

© 2017 The Authors. Published by Elsevier B.V. This is an open access article under the CC BY license (<http://creativecommons.org/licenses/by/4.0/>). Funded by SCOAP<sup>3</sup>.

\* Corresponding author.

E-mail address: [paul.john.davies@gmail.com](mailto:paul.john.davies@gmail.com) (P.J. Davies).

## 1. Introduction

The region around  $^{100}\text{Sn}$  is the location of a fascinating variety of physical phenomena [1–5]. For example, recent experimental work on  $^{100}\text{Sn}$  measured the largest Gamow Teller (GT) strength for an allowed  $\beta$ -decay [6], the low lying levels of  $^{92}\text{Pd}$  [7] and the high spin isomeric state in  $^{96}\text{Cd}$  [2] highlight the importance of the isoscalar ( $T = 0$ ) proton–neutron ( $pn$ ) interaction on energy levels in self-conjugate nuclei in the region, and the proximity of the  $N = Z = 50$  shell closure leads to a significant number of both spin-gap and seniority isomers, e.g., see [2,4,5,8–13]. These rather different nuclear structure features provide an ideal testing ground for shell model effective interactions and model spaces. In particular, the experimental and theoretical investigation of isomeric states has contributed significantly to our understanding of the nuclear structure as well as our abilities to predict nuclear properties in this region of the nuclear chart.

The key active orbitals ( $p_{1/2}$ ,  $g_{9/2}$ ) for the  $N \approx Z$  nuclei in the mass 90 region are expected to be well isolated, which made the empirical shell model (ESM) a particularly attractive tool for interpreting the structure of excited states [14–16]. Away from the  $N = Z$  line it has been demonstrated that such calculations can provide a good description of low energy states and that a dominant  $g_{9/2}$  orbital leads to both spin-gap and seniority isomers [2, 8–13]. The spin-gap isomers arise from the strong attraction between neutrons and protons occupying this orbital. In some nuclei this can produce states with lifetimes long enough to give significant  $\beta$ -decay branches [17–19]. Furthermore, the large  $Q_{\beta^+}$  values for these states often allows a significant part of the GT strength to be probed. Since the GT strength is related to the overlap between the initial and final wave functions, studies of such isomer decay properties can provide a sensitive test of shell model interactions. An area of particular interest in recent years has been the high-spin isomeric states in  $N \approx Z$  nuclei, where recent experimental work has tested the suitability of different shell model spaces. Examples include:  $^{94}\text{Pd}$  [5],  $^{94}\text{Ag}$  [9,13],  $^{96}\text{Ag}$  [4],  $^{98}\text{Cd}$  [3], where the  $pg$  ( $p_{1/2}$ ,  $g_{9/2}$ ),  $fp_g$  ( $f_{5/2}$ ,  $p_{3/2}$ ,  $p_{1/2}$ ,  $g_{9/2}$ ), and  $gds$  ( $g_{9/2}$ ,  $g_{7/2}$ ,  $d_{5/2}$ ,  $d_{3/2}$ , and  $s_{1/2}$ ) model spaces have been used to explain the observed isomers.

$^{96}\text{Cd}$  is the last even–even  $N = Z$  nucleus before  $^{100}\text{Sn}$ . The most recent work on this nucleus identified the  $16^+$  spin gap isomer, measuring the lifetime and  $B(\text{GT})$  strength [2,20]. By performing shell model calculations using the GF interaction [16], it was demonstrated that the  $T = 0$   $pn$  interaction plays an important role in explaining the isomerism of this state. LSSM calculations presented in the same study, which employed an effective interaction for the  $gds$  model space, predicted the existence of three high-lying resonance-like states that reside  $\sim 5$  MeV above the proton separation energy in the daughter nucleus  $^{96}\text{Ag}$  [2]. This work suggested that  $\sim 30\%$  of the  $\beta$  decay strength from the  $16^+$  isomer should populate these resonance-like states and hence the observation of  $\beta$ -delayed protons might be expected. However, due to limited statistics no protons (or  $\gamma$  rays) from the decay of these resonance-like states were detected in the previous experiment [2]. Additionally, the deduced  $B(\text{GT})$  strength for the  $\beta$  decay of  $^{96}\text{Cd}$  was found to be consistent with that calculated using both interactions. Identification of a  $\beta$ -delayed proton branch along with detailed  $\gamma$  ray spectroscopy would yield valuable information on the validity of the LSSM calculations as well as providing important information on the wavefunction of the  $16^+$  isomer.

In this letter we report evidence for the existence of the  $\beta$ -delayed proton branch from the decay of the  $16^+$  isomer in  $^{96}\text{Cd}$  along with the observation that this predominantly populates the  $25/2^+$  and  $29/2^+$  states in  $^{95}\text{Pd}$ . LSSM calculations, using the  $gds$  model space, in combination with new WKB estimates for the pro-

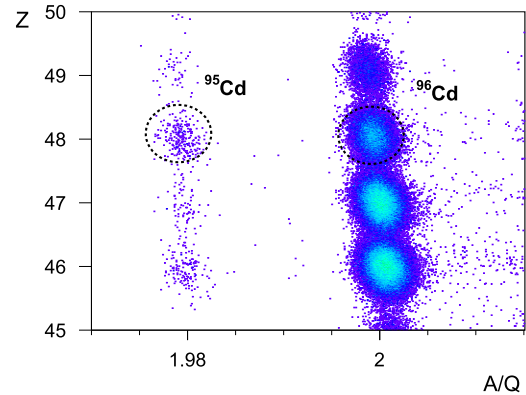


Fig. 1. The particle ID for ions transmitted through BigRIPS and identified as being implanted in the active stopper (AS).

ton emission probability, reveal the importance of the core excited orbitals in the wavefunction of the  $16^+$  spin-gap isomer. Also reported are improved lifetime measurements for the ground state and  $16^+$  isomer in  $^{96}\text{Cd}$ , as well as the lifetime of the ground state of  $^{95}\text{Cd}$ .

## 2. Experiment

A secondary cocktail beam, which included the nuclide of interest  $^{96}\text{Cd}$ , was produced by the Radioactive Ion Beam Factory (RIBF) at the RIKEN Nishina Centre, by in-flight fragmentation of a primary beam of  $^{124}\text{Xe}$ . The primary beam, at an energy of 345 A MeV, was incident on a  $^9\text{Be}$  target of areal density  $740 \text{ mg cm}^{-2}$  and BigRIPS [21,22] was employed to separate the resulting fragments. Identification of fragments in the secondary beam was done event-by-event; particle tracking combined with the magnetic rigidity of BigRIPS is used to obtain time-of-flight measurements and determine  $A/Q$ , whilst the energy loss in an ionisation chamber was used for  $Z$  identification (see Fig. 1). Ions of interest were implanted in the active stopper (AS) SIMBA [6], located at the end of the zero degree spectrometer [22].

SIMBA was constructed from three double sided silicon strip detectors (DSSSD) arranged in a stack along the direction of the beam. Each detector had 40 strips of 1 mm pitch on the upstream side and 60 strips of the same pitch on the downstream side, providing a total of 7200 pixels. The three DSSSD's in the AS were 1 mm thick, these DSSSD's provided good  $\beta$ -proton discrimination for the decays of interest. A thinner DSSSD, read out with a XY resistor chain, located upstream of the AS was employed to track the position of incoming heavy ions, and used in conjunction with the DSSSD to determine the implantation pixel. In addition, a  $\beta$ -particle calorimeter was located downstream of the AS. This was composed of a stack of 16 silicon detectors, sandwiched between 4 single sided silicon strip detectors (SSSSD), 2 arranged to provide x and y strips upstream of the stack of 16 silicon detectors and the other 2 located in the same configuration down stream. The SSSSD allowed  $\beta$  particles to be tracked through the calorimeter, in addition they also acted as a veto on heavy ions which were not stopped by the AS. Surrounding the AS was the EUROBALL-RIKEN Cluster Array (EURICA), which contained 84 large volume HPGe detectors [23,24].

All events were time stamped and in the offline analysis decays were correlated, in time and position, with either the most recent implant in the same pixel and within a fixed period of time or all implants that occurred within the previous 60 s, chosen to cover the daughter and granddaughter decays. The first correlation procedure produces clean  $\beta$  and  $\beta p$  delayed  $\gamma$  ray spectra at the

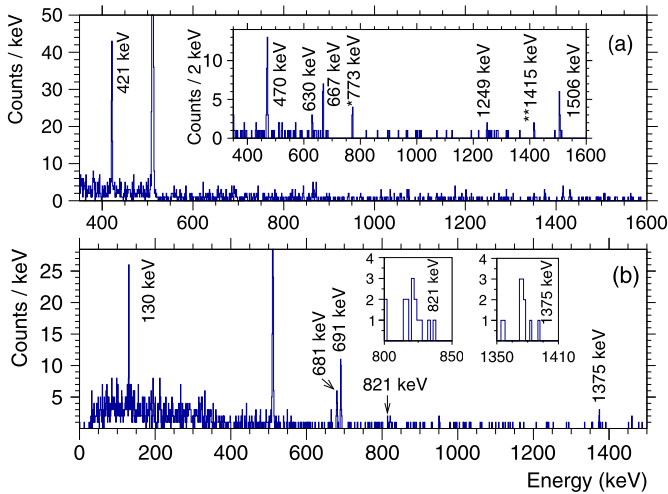


**Fig. 2.** (a)  $\gamma$ -rays emitted in prompt coincidence (0–200 ns) following the detection of  $\beta$  particles and (inset)  $\gamma$ -rays emitted between 0.2 and 4  $\mu$ s after detection of the  $\beta$  particle. The  $\gamma$  ray marked with a \*773 keV is the  $4^+ \rightarrow 2^+$  in  $^{92}\text{Mo}$  and is attributed to correlations with the time random background, the  $2^+ \rightarrow 0^+$  (transition not labelled) is also present at 1510 keV, the \*\*1415 keV is the decay from the  $2^+ \rightarrow 0^+$  in the granddaughter  $^{96}\text{Pd}$ . (b)  $\gamma$ -rays emitted in prompt coincidence following the detection of a  $\beta$  delayed proton (insets left and right show the 821 keV and 1375 keV transitions, respectively). In both cases the decay events are uniquely correlated to the previous  $^{96}\text{Cd}$  ion implanted in the same pixel, using the method discussed in section 2, and using a  $\beta$  correlation time of 1.35 s, which is three half lives of the  $16^+$  isomer deduced in the current work.

expense of correlation efficiency. In the latter correlation procedure the efficiency is improved and allows for a good measurement of the time random background, the background introduced by the daughter and granddaughter decays can be accounted for using values for the half-lives already published. The geometric efficiency for the detection of  $\beta$  particles and protons was determined using a Geant4 simulation [25]. These were found to be  $\sim 30(5)\%$  in the case of  $\beta$ -ion correlations and  $\sim 92(10)\%$  for  $\beta p$ -ion correlations.

### 3. Results

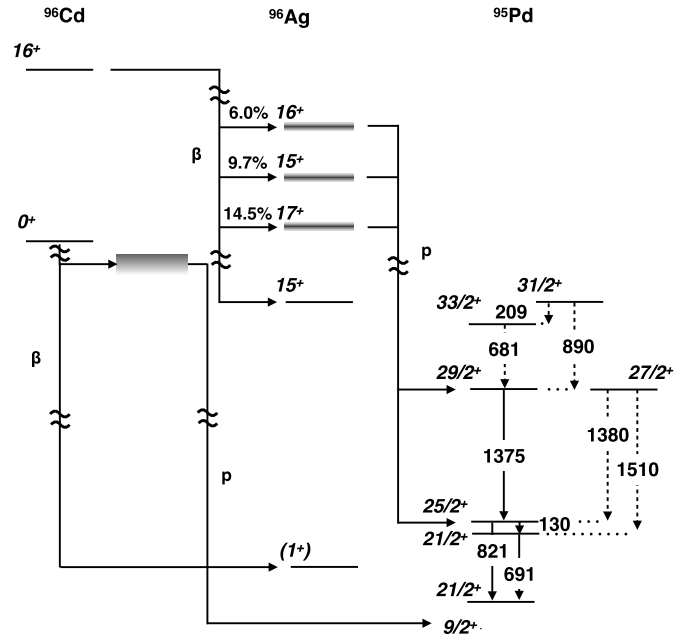
In total 17,000 ions of  $^{96}\text{Cd}$  were transmitted through BigRIPS and implanted into the AS of the decay station. An energy threshold of 2 MeV was used to differentiate between  $\beta$  and  $\beta p$  decays, whilst a lower energy threshold of 150 keV was used for  $\beta$  decays. The 2 MeV threshold represents a suitable lower limit for summed  $\beta p$  events and was determined using the Geant4 simulation discussed in section 2 [25]. Fig. 2(a) shows both prompt- $\gamma$  and delayed- $\gamma$  spectra following  $^{96}\text{Cd}$  ion- $\beta$  detection. In the main part of Fig. 2(a) prompt  $\gamma$  ray events between 0 and 200 ns after a  $\beta$ -decay event in the AS are presented, whilst the inset shows  $\gamma$  rays emitted between 0.2 and 4  $\mu$ s after the  $\beta$  decay. The  $\gamma$  rays observed in the inset spectrum at 470, 630, 667, 1249 and 1506 keV are from the known decay of the  $15^+$  isomer in  $^{96}\text{Ag}$  [2, 4], and the 421 keV  $\gamma$  ray in Fig. 2(a) has been previously assigned as being due to the decay of a low-lying  $1^+$  state in  $^{96}\text{Ag}$  [2].

Fig. 2(b) shows  $\gamma$  rays emitted between 0 and 200 ns after the identification of  $\beta$  delayed proton events in the AS that are correlated with an implanted  $^{96}\text{Cd}$  ion. The  $\gamma$  rays observed at 130, 691, 821, and 1375 keV are known to form a decay sequence which populates the  $21/2^+$  isomer in  $^{95}\text{Pd}$  [11]. A further  $\gamma$ -ray can be seen in Fig. 2(b) at 681 keV,  $\gamma$  rays of this energy exist in both  $^{95}\text{Rh}$  [20] and  $^{95}\text{Pd}$  [11,12], which are the  $\beta p$  daughters of  $^{96}\text{Ag}$  and  $^{96}\text{Cd}$ , respectively. The time distribution of this  $\gamma$  ray, and an estimate of the intensity expected for the known  $\beta p$  decay of  $^{96}\text{Ag}$  within the  $\beta$  correlation window (1.35 s) used to construct

**Table 1**

Observed, efficiency corrected,  $\gamma$  ray energies and intensities for transitions in  $^{95}\text{Pd}$  following the  $\beta p$  decay of  $^{96}\text{Cd}$ . The intensities are normalised to the 130 keV transition intensity, which has been set at 100% (electron conversion coefficient has not been included in the calculation of these intensities).

$E_\gamma$	$I_i \rightarrow I_f$	$I_\gamma$
691	$\frac{23}{2}^+ \rightarrow \frac{21}{2}^+$	91(28)
130	$\frac{25}{2}^+ \rightarrow \frac{23}{2}^+$	100(19)
821	$\frac{25}{2}^+ \rightarrow \frac{21}{2}^+$	36(19)
1375	$\frac{29}{2}^+ \rightarrow \frac{25}{2}^+$	81(36)



**Fig. 3.** Proposed decay scheme for the  $\beta$  decay and  $\beta p$  decay of the  $16^+$  isomer in  $^{96}\text{Cd}$ , the transitions marked with dashed lines were not observed but are within the available angular momentum of the proton decay. The calculated branching ratios to the GT resonance states in  $^{96}\text{Ag}$ , extracted from LSSM calculations, are also presented. The partial decay scheme of  $^{95}\text{Pd}$  was taken from [11].

the spectrum, indicate that all the events for this transition correspond to the  $\beta p$  delayed  $\gamma$  ray from  $2^+$  state in  $^{96}\text{Ag}$  [20,26]. These events are present in the spectrum because of the low  $\beta$  correlation efficiency, which results in a reasonable probability of missing the first  $\beta$  event and detecting a subsequent event from the daughter.

The intensities of the  $\gamma$  rays identified as being in  $^{95}\text{Pd}$  are presented in Table 1 and a decay scheme showing the states populated in the current work is presented in Fig. 3. Also included in this figure are the  $27/2^+$ ,  $31/2^+$  and  $33/2^+$  states in  $^{95}\text{Pd}$ , the non-observation of  $\gamma$ -rays from these states eliminates some potential decay pathways.

A time distribution of events between the implantation of a  $^{96}\text{Cd}$  ion and its decay (dT) was obtained for the  $16^+$  spin gap isomer by gating on the  $\beta$  and  $\beta p$  delayed  $\gamma$  rays. The Schmidt method was then employed to fit the time distribution, see Fig. 4(a), this result is presented in Table 2 where it is compared to the previously measured value. The implantation rate precluded performing the same analysis for the ground state. In this case the half-life was extracted by allowing it to be a free parameter in the fits of the  $\beta$ -decay time distributions discussed in the next paragraph and presented in Fig. 4(d). Also presented in

**Table 2**

Experimental half-life measurements for  $^{95,96}\text{Cd}$  obtained in the current work compared to experimental and theoretical values from the literature. The B(GT) and  $\beta p$  ( $I_{\beta p}$ ) branching ratios for  $^{96}\text{Cd}$ , determined in the present work, are compared to experimental values from the literature. The Isomeric ratio from the present work is presented.

Nucleus	$I_i^\pi$	Half lives (s)			B(GT)		$I_{\beta p}$		Isomeric ratio
		This work	Literature	Theory	This work	Literature	This work	Literature	
$^{96}\text{Cd}_g$	$0^+$	0.97(9)	0.67(15) <sup>a</sup> 1.03 <sup>+0.24</sup> <sub>-0.21</sub> <sup>b</sup>	2.18 <sup>d</sup>	–	–	1.5(5)%	5.5(40)% <sup>b</sup>	–
$^{96}\text{Cd}_m$	$16^+$	0.45 <sup>+0.05</sup> <sub>-0.04</sub>	0.29 <sup>+0.11</sup> <sub>-0.10</sub> <sup>a</sup>	0.5 <sup>e</sup>	<0.11(2) <sup>c</sup>	0.19 <sup>+0.10</sup> <sub>-0.06</sub> <sup>a</sup>	11(3)%	–	48(15)%
$^{95}\text{Cd}$	(9/2 <sup>+</sup> )	0.029(8)	–	0.0317 <sup>d</sup>	–	–	–	–	–

<sup>a</sup> From Ref. [2].

<sup>b</sup> From Ref. [26].

<sup>c</sup> Upper limit for the decay into the  $15^+$  state in  $^{96}\text{Ag}$ .

<sup>d</sup> From Ref. [32].

<sup>e</sup> From Ref. [17].

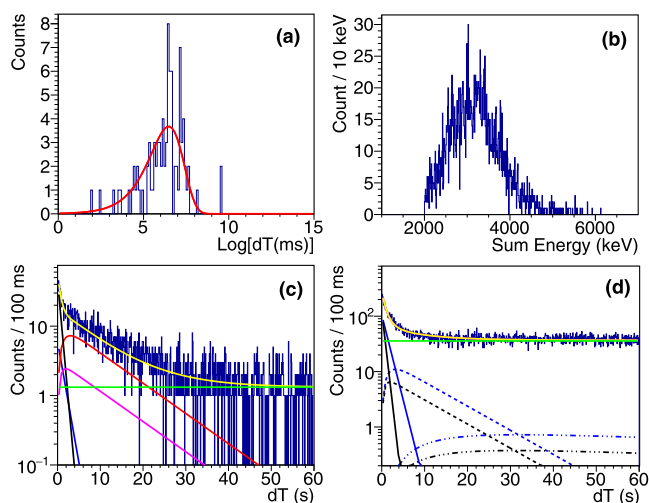


**Fig. 4.** (a) Sum of natural log(dT) for all  $\beta$ - and  $\beta p$ -delayed  $\gamma$ -rays observed after the decay of the  $16^+$  spin gap isomer in  $^{96}\text{Cd}$ , where dT is the time between a correlated implant and decay event. The red line is the result of a fit using the Schmit method which yields a mean lifetime (half-life) of  $649_{-59}^{+72}$  ms ( $450_{-43}^{+53}$  ms). (b) Sum energy recorded in the active stopper SIMBA, for  $\beta$ -delayed proton events in coincidence with  $^{96}\text{Cd}$  implanted ions. (c) Time distributions of  $\beta$ -delayed proton events in coincidence with  $^{96}\text{Cd}$  ions. All implantation events found within a time window of 60 s prior to the decay were correlated. The fit result is shown in yellow, the individual components, parent ( $^{96}\text{Cd}(16^+)$ : black,  $^{96}\text{Cd}(0^+)$ : blue), daughter ( $^{96}\text{Ag}(8^+)$ : pink,  $^{96}\text{Ag}(2^+)$ : red), background (green), are also shown. (d) same as (c) except for  $\beta$ -decay events, the fit result is shown in yellow, the individual parents are solid lines ( $^{96}\text{Cd}(16^+)$ : black,  $^{96}\text{Cd}(0^+)$ : blue), daughters are dashed lines ( $^{96}\text{Ag}(8^+)$ : black,  $^{96}\text{Ag}(2^+)$ : blue), and granddaughters are dot-dashed lines ( $^{96}\text{Pd}(0^+)$ : black/blue). (For interpretation of the references to colour in this figure, the reader is referred to the web version of this article.)

Table 2 is the first measurement of the half-life of  $^{95}\text{Cd}$  which has been deduced from the current work.

The  $\beta p$  branching ratio for the decay of the  $16^+$  isomer and the ground state were determined from statistical fits to the time distributions. The distributions were produced by requiring a correlation between an implanted  $^{96}\text{Cd}$  ion and all decays within 60 s, observed in the same pixel, as described in section 2. The fits for  $\beta p$ - and  $\beta$ -decay are presented in Figs. 4(c) and (d) respectively. In both cases the half-life of the  $16^+$  isomer was fixed to the value established in the present work, whilst the ground state half-life remained a free parameter, the half-lives of the daughter states were fixed to the currently accepted values in the literature [4, 11, 12, 20, 26]. In the case of  $\beta$ -decay exponential fit components for the parent, daughter and granddaughter were included along with a linear component for the time random background. For the  $\beta$ -delayed proton branch the analysis is complicated by the finite efficiency of  $\beta$  detection coupled to large  $\beta p$  branches in the daughter nucleus  $^{96}\text{Ag}$  [20, 26]. To account for this  $\beta\beta$ -delayed

proton branch exponential functions for the daughter, with initial values that were independent of the parent decay, were included along with the exponential function for the parent decay. In both cases, and in order to reduce the number of free parameters in the fit, the magnitude of the time random background was established by fitting a constant function between 50 and 60 s after the ion is implanted. This region is expected to be dominated by time random correlations. The relative efficiency between  $\beta$  and proton detection was established with the detailed Geant4 simulation [25]. The resulting experimental  $\beta p$  branching ratios for both the  $16^+$  isomer and the ground state are presented in Table 2. Fig. 4(b) shows the energy distribution of the  $\beta$ -delayed protons.

#### 4. Discussion

Previous experiments have looked at the  $\beta$  decay of  $^{96}\text{Cd}$  [2, 20, 27]. The work of Bazin et al. measured the half-life of the ground state decay as  $1.03_{-0.21}^{+0.24}$  s, but found no evidence of the decay of the predicted  $16^+$  isomer [27]. However, the MLH method of analysis used in their work did not rule out such an isomer existing. The first evidence for the existence of the  $16^+$  isomeric state in  $^{96}\text{Cd}$  was presented by Nara Singh et al., where the high spin state was identified through the observation of  $\beta$ -delayed  $\gamma$ -rays following population of the  $15^+$  isomeric state in the daughter nucleus  $^{96}\text{Ag}$  [2]. In the latter work the half-life of the ground state was measured as 0.67(15) s and that of the  $16^+$  isomer was reported as  $0.29_{-0.10}^{+0.11}$  s. The half-lives determined from the current work, see Table 2, are consistent with both previous measurements, but with improved precision.

In the current work a  $\beta p$  decay branch of the  $16^+$  spin-gap isomer in  $^{96}\text{Cd}$  has been identified. It is clear from Fig. 2(b) that  $\gamma$  rays from four states in  $^{95}\text{Pd}$  are observed. The efficiency corrected  $\gamma$  ray intensities, are presented in Table 1. Fig. 2(b) indicates that there is no evidence, within the levels of statistics obtained in the present experiment, for any significant population of the  $33/2^+$ ,  $31/2^+$  or  $27/2^+$  states in  $^{95}\text{Pd}$  (see discussion in sect. 3 regarding the 681 keV transition). Fig. 3 shows a decay scheme for the observed  $\gamma$  decays in the  $\beta p$  daughter  $^{95}\text{Pd}$ . Although a small  $\beta p$  decay branch is reported in the present work for the decay of the ground state no  $\gamma$  rays belonging to  $^{95}\text{Pd}$  are observed in coincidence with this decay branch.

Shell model calculations employing the Gross–Frenkel (GF) effective interaction [16], which employs the  $\pi\nu(p_{1/2}, g_{9/2})$  shell model orbitals, were previously reported in [2] to show that the two body matrix element for the  $T=0$   $pn$  pairs are fundamental in explaining the isomerism of the  $16^+$  state. The same work reported the results of LSM calculations for both  $^{96}\text{Cd}$  and  $^{96}\text{Ag}$ , using the larger  $gds$  model space and allowing 4-particle–4-hole (4 p–h) ( $^{96}\text{Cd}$ ,  $t=4$ ) and 5 p–h ( $^{96}\text{Ag}$ ,  $t=5$ ) excitations. These shell model calculations show that the wavefunction of the

**Table 3**  
Results of shell model calculations performed in the present and previous work [2] and WKB estimates for proton decays from the three GT resonances in  $^{96}\text{Ag}$ . The table gives estimates for  $\beta\gamma$  and  $\beta p$  decay probabilities from the resonant like states in  $^{96}\text{Ag}$ , showing the centroid of the  $I_\beta$  distribution ( $E_{res}$ ), percentage population expected by the  $\beta + \text{EC}$  decay of the  $16^+$  isomer in  $^{96}\text{Cd}$  ( $I_\beta$ ),  $\gamma$  ray multipolarity ( $\sigma L$ ),  $\gamma$  ray energy ( $E_\gamma = E_{res} - E_x(15^+)$ ),  $\gamma$  ray decay width ( $\Gamma_\gamma$ ), centroid proton emission  $Q$  value ( $Q_p$ ) to  $^{95}\text{Pd}$  states, WKB proton emission decay width weighted by the spectroscopic factor ( $\Gamma_p$ ) for the  $\ell = 0, 2, 4$  proton emission, spin and parity of the final state populated in proton emission ( $I_{fin}^\pi$ ), and the  $\beta p$  branch from the decay of the  $16^+$  state in  $^{96}\text{Cd}$  ( $I_{\beta p}$ ). Only the states with the strongest population are shown.

$I_{res}^\pi$	$E_{res}$ MeV	$I_\beta$ %	$\sigma L$	$E_\gamma$ MeV	$\Gamma_\gamma$ meV	$Q_p$ MeV	$\Gamma_p$ (meV)			$I_{fin}^\pi$	$I_{\beta p}$ %
							$\ell = 0$	$\ell = 2$	$\ell = 4$		
$15^+$	9.11	9.7	M1/E2	6.49	60	3.09	23	115	0.1	$29/2^+$	<0.1
							4.46	8930	13.2	$25/2^+$	9.7
$16^+$	9.34	6.0	M1/E2	6.72	160	3.32	–	361	1.3	$29/2^+$	3.1
							3.32	180	0.6	$27/2^+$	1.5
$17^+$	8.82	14.5	M1/E2	6.20	25	2.80	–	55	0.2	$29/2^+$	10.2

$16^+$  isomer in the parent nucleus  $^{96}\text{Cd}$  contains only 76% of the ( $\pi g_{9/2}^{-2}, \nu g_{9/2}^{-2}$ ) configuration (the remainder involving core excited components). The same calculations also predict the existence of  $15^+$ ,  $16^+$ , and  $17^+$  resonance-like states, involving core-excited neutron configurations, in the daughter nucleus  $^{96}\text{Ag}$  at energies of 10.2 MeV, 10.6 MeV, and 9.5 MeV, respectively. The energies of these states were extracted from the centroids of the B(GT) distributions. The core excited states were described as GT resonances since they reside above the proton separation energy and have a width of approximately 2 MeV. As such they are expected to have a reasonably large proton decay branch. A prediction of 32% was made for the  $\beta$  decay branch from the  $16^+$  spin-gap isomer to the GT resonances states. Furthermore, simple WKB estimates were performed using a square well potential, and assuming a spectroscopic factor of 0.1 for the decay of an  $\ell = 0$  proton from the GT resonances [2]. In addition, B(M1) and B(E2) strengths of 1 W.u. were assumed for the  $\gamma$  decay of these states. The results of these calculations indicated that the GT resonances should decay via both  $\gamma$  and proton branches in a ratio of  $\sim 2:1$ , respectively.

Based on the previous LSSM calculations [2] and new shell model calculations the  $\beta p$  decay of the  $16^+$  spin gap isomer in  $^{96}\text{Cd}$  was studied. From the LSSM, the three GT resonance spins ( $I_{res}^\pi$ ), centroids ( $E_{res}$ ) of the  $\beta + \text{EC}$  feeding distributions, feeding percentage ( $I_\beta$ ), total  $\gamma$  decay energy ( $E_\gamma$ ) to the  $15^+$  state in  $^{96}\text{Ag}$ , and the proton decay  $Q$  values to the yrast  $I^\pi = (25/2 - 29/2)^+$  states in the daughter  $^{95}\text{Pd}$  were inferred. The results of these calculations are listed in columns 1 to 3 and 5, 7 of Table 3. Proton emission to lower and higher spin states were calculated but found to be negligible due to decay energy or spectroscopic strength, hence they are not listed. A shell model based estimate for  $\beta\gamma$  and  $\beta p$  ratios requires the knowledge of B(M1) and B(E2) strengths from resonance states to valence and core excited states, and of spectroscopic factors from resonance states to  $^{95}\text{Pd}$  daughter states. To determine these, simplified shell model calculations have been performed in the  $gds$  model space, these allow one-particle one-hole excitations (i.e.  $t_\pi = t_\nu = 1$  truncation), including simultaneous proton and neutron excitations, across the  $N = Z = 50$  closed shells. In the case of the hole-hole (h-h) configurations, which are dominated by the  $g_{9/2}$  valence space, the interaction was taken from  $fp_g$  calculations [4,5]. Whilst for the cross shell particle-hole (p-h) configurations, two body matrix elements from the SNA interaction in the OXBASH program package were employed, which are taken from the H7B potential [28]. From the results, GT transitions for the decay of the  $^{96}\text{Cd}$   $16^+$  isomer to the GT resonances in  $^{96}\text{Ag}$  were calculated, as were the B(M1) and B(E2) values for the decay from the GT resonances in  $^{96}\text{Ag}$  to the isomeric  $15^+$  state and spectroscopic factors (SF) for the decay of the GT resonance states to the  $25/2^+$ ,  $27/2^+$ ,  $29/2^+$ ,  $31/2^+$ , and  $33/2^+$  states in  $^{95}\text{Pd}$ , which the LSSM calculations show have very little of the core excited configurations. The effect of the truncation on excitation energies of the GT resonances was compensated

for by a monopole correction so the centroids sit at the same energy as the  $t = 5$  LSSM calculations presented by Nara Singh et al. [2]. The  $\Gamma_p$  penetration widths were calculated in accordance with the prescription given in Ref. [29] and weighted by the appropriate spectroscopic factor. The  $\Gamma_\gamma(M1)$ ,  $\Gamma_\gamma(E2)$  and  $\Gamma_p$  widths are determined by averaging over the four strongest fed  $15^+$ ,  $16^+$ , or  $17^+$   $\beta^+/\text{EC}$  states in  $^{96}\text{Ag}$ . A final point to note is the energies of these resonance-like states were determined from the centroid of the  $I_\beta$  distribution which has the effect of lowering their energy by approximately 1 MeV with respect to the previously published LSSM calculations [2].

It is clear from Table 3 that the decay from the GT resonances to both the  $25/2^+$  and  $29/2^+$  states in  $^{95}\text{Pd}$  are favoured by  $Q$ -value ( $Q_p$ ), barrier penetration probabilities or spectroscopic factor ( $\Gamma_p$ ). All decays proceed primarily via  $\ell = 2$  proton emission, which is favoured over  $\ell = 4$ , due to the centrifugal barrier, and over  $\ell = 0$ , due to the spectroscopic factor. The results of the calculations are in fair agreement with the experimental results, where the observed  $\gamma$ -ray intensities suggest that both the  $25/2^+$  and  $29/2^+$  states are favoured by the  $\beta p$  decay of the  $16^+$  isomer in  $^{96}\text{Cd}$ . The calculated  $Q_p$  values also agree nicely with the average value for the  $\beta p$  decay energy, which is shown in the inset of Fig. 4(b). The dominance of the  $\ell = 2$  proton emission from the GT resonances in  $^{96}\text{Ag}$  highlights the importance of core excited orbitals in the wavefunction of the  $16^+$  isomer in  $^{96}\text{Cd}$ . A comparison of  $\Gamma_p$  to the  $\Gamma_\gamma$  decay widths in Table 3 highlights a further interesting feature of the present calculations, which is that the  $\ell = 2$  proton emission appears to dominate the decay of GT resonances compared to the  $\gamma$  decay branches. Whilst noting the limitations of the calculations indicated, the calculated branching ratio suggests that less than 6% of decays from the GT resonances proceed via the  $\gamma$  decay branch. This in turn results in a  $\beta p$  branching ratio for the  $16^+$  state in  $^{96}\text{Cd}$  of approximately 25%, which is comparable to the experimental result of 11(3)% obtained from the current work. The theoretical value of 25% is an upper limit, Table 3 only includes M1 and E2 transitions as E1 can not be calculated in the  $gds$  model space. Hence, the total calculated  $\Gamma_\gamma$  width represents a lower limit. In general both proton and  $\gamma$ -ray decay modes are rather sensitive to small components of the wave functions, with typical values of B(M1)  $\sim 2.5 \times 10^{-3}$  W.u., B(E2)  $\sim 2.5 \times 10^{-2}$  W.u., and SF  $\sim 1.5 \times 10^{-3}$ . This is due to the fact that the GT daughter states are dominated by neutron core excitation while the  $\gamma$ - and  $p$ -decay final states are mainly valence  $g_{9/2}^n$  states with comparatively little core excitation. However, the importance of  $\ell = 2$  proton emission seems well established by the current work.

The B(GT) strength for a  $\beta$  decay can act as a sensitive probe of nuclear structure effects. This was calculated using  $B(GT) = \frac{3860(18)I_\beta}{f t_{1/2}}$ , where  $I_\beta$  is the  $\beta$  decay branching ratio,  $f$  is the phase space factor tabulated for various nuclei [2,30]. The non-observation of gamma ray branches from the GT resonances means that these are most likely composed of many individual states,

most commonly called the pandemonium effect [31], and only the combined B(GT) strengths can be determined. Nevertheless, an upper limit for the B(GT) for the decay from the  $16^+$  isomer in  $^{96}\text{Cd}$  to the  $15^+$  isomer in  $^{96}\text{Ag}$  can be obtained by taking the  $\beta p$  branch of 11(3)% as the lower limit of the decay to the GT resonance states in the daughter  $^{96}\text{Ag}$ . With this assumption it is possible to establish an upper limit of  $B(\text{GT} : ^{96}\text{Cd}(16^+) \rightarrow ^{96}\text{Ag}(15^+)) < 0.11(2)$ , using  $t_{1/2} = 450^{+53}_{-43}$  ms,  $Q_{EC} = 11.51(26)$  MeV [2], and  $I_{\beta} = 89(5)\%$ , for the decay to the  $15^+$  isomer. The B(GT) deduced above for the decay to the  $15^+$  isomer in  $^{96}\text{Ag}$  is consistent with the value of  $B(\text{GT}) = 0.19^{+0.10}_{-0.06}$  previously reported for this nucleus [2]. The currently revised upper limit is also in agreement with the predictions from the previous LSSM calculations[2], which produced a B(GT) value of 0.07 for this decay. However, as noted in the previous paragraph, the proton emission is expected to dominate the decay of the GT resonances in  $^{96}\text{Ag}$ , if this is the case then the pandemonium effect will have only a marginal effect on the measured value presented in the current work. At present it is unclear as to the role of  $\gamma$  decay from the GT resonances in  $^{96}\text{Ag}$ . What is clear is that the  $16^+$  state in  $^{96}\text{Cd}$  has a significant  $\beta p$  decay branch, the size of which is very sensitive to the location of high lying GT resonance states in  $^{96}\text{Ag}$ . These states are dominated by p–h excitations across the  $Z = 50$  shell gap, demonstrating the importance of such correlations in this region.

## 5. Summary

In summary, the  $\beta p$  decay branch from the  $16^+$  isomer in  $^{96}\text{Cd}$  has been observed for the first time in the present work. More precise values for the half-life of the ground state and  $16^+$  spin gap isomer are presented, along with the measurement of the ground state half-life of  $^{95}\text{Cd}$ .  $\beta p$  delayed  $\gamma$  ray spectra show that high spin states are populated in the granddaughter nucleus  $^{95}\text{Pd}$ , with the most prominent decay paths populating both the  $25/2^+$  and  $29/2^+$  states in  $^{95}\text{Pd}$ . LSSM calculations for  $^{96}\text{Ag}$ , the  $\beta$  decay daughter of  $^{96}\text{Cd}$ , show the presence of GT resonance states resulting from p–h excitations across the  $N = Z = 50$  shell gap. WKB estimates coupled to B(M1) and B(E2) decay strength calculations suggest an upper limit for the  $\beta p$  branching ratio of 25%, in reasonable agreement with the experimentally obtained value of 11(3)%. An upper limit of 0.11(2) is deduced for the B(GT)  $\beta$  decay

strength to the  $15^+$  isomer in  $^{96}\text{Ag}$ . The present work highlights the importance of wavefunction components from core excited orbitals in the  $16^+$  spin gap isomer in  $^{96}\text{Cd}$ .

## Acknowledgements

This work was partially supported by the German BMBF grant 05P12PKFNE, the UK Science and Technology Facilities Council (STFC) grants ST/J000124/1 and ST/L005727/1, and the U.S. DOE grant DE-FG02-91ER40609.

## References

- [1] T. Faestermann, M. Górska, H. Grawe, Prog. Part. Nucl. Phys. 69 (2013) 85.
- [2] B.S. Nara Singh, et al., Phys. Rev. Lett. 107 (2011) 172502.
- [3] A. Blazhev, et al., J. Phys. Conf. Ser. 205 (2010) 2035.
- [4] P. Boutachkov, et al., Phys. Rev. C 84 (2011) 044311.
- [5] T.S. Brock, et al., Phys. Rev. C 82 (2010) 061309.
- [6] C.B. Hinke, et al., Nature 486 (2012) 341.
- [7] B. Cederwall, et al., Nature 469 (2011) 7328.
- [8] J. Döring, et al., Phys. Rev. C 68 (2003) 034306.
- [9] M. La Commara, et al., Nucl. Phys. A 708 (2002) 167.
- [10] G. Lorusso, et al., Phys. Lett. B 699 (2011) 141.
- [11] R. Marginean, et al., Phys. Rev. C 86 (2012) 034339.
- [12] N. Marginean, et al., Phys. Rev. C 67 (2003) 061301.
- [13] C. Plettner, et al., Nucl. Phys. A 733 (2004) 20.
- [14] F.J.D. Serduke, R.D. Lawson, D.H. Gloeckner, Nucl. Phys. A 256 (1976) 45.
- [15] D.H. Gloeckner, F.J.D. Serduke, Nucl. Phys. A 220 (1974) 477.
- [16] R. Gross, A. Frenkel, Nucl. Phys. A 267 (1976) 85.
- [17] K. Ogawa, Phys. Rev. C 28 (1983) 958.
- [18] M. Górska, et al., Z. Phys. A 353 (1995) 233.
- [19] E. Nolte, G. Korschinek, U. Heim, Z. Phys. A 298 (1980) 191.
- [20] L. Batist, et al., Nucl. Phys. A 720 (2003) 245.
- [21] T. Kubo, Nucl. Instrum. Methods Phys. Res., Sect. B, Beam Interact. Mater. Atoms 204 (2003) 97.
- [22] T. Kubo, et al., Prog. Theor. Exp. Phys. 2012 (2012) 03C003.
- [23] S. Pietri, et al., Nucl. Instrum. Methods Phys. Res., Sect. B, Beam Interact. Mater. Atoms 261 (2007) 1079.
- [24] P.A. Söderström, et al., Nucl. Instrum. Methods Phys. Res., Sect. B, Beam Interact. Mater. Atoms 317 (2013) 649.
- [25] N. Warr, A. Blazhev, K. Moschner, EPJ Web Conf. 93 (2015) 07008.
- [26] G. Lorusso, et al., Phys. Rev. C 86 (2012) 014313.
- [27] D. Bazin, et al., Phys. Rev. Lett. 101 (2008) 252501.
- [28] A. Hosaka, et al., Nucl. Phys. A 444 (1985) 76.
- [29] A. Gillitzer, et al., Z. Phys. A 326 (1987) 107.
- [30] N.B. Gove, M.J. Martin, At. Data Nucl. Data Tables 10 (1971) 205.
- [31] J.C. Hardy, L.C. Carraz, B. Jonson, P.G. Hansen, Phys. Lett. B 71 (1977) 307.
- [32] H. Herndl, B.A. Brown, Nucl. Phys. A 627 (1997) 35.